Journal of Controlled Release 159 (2012) 302–308

Contents lists available at SciVerse ScienceDirect

Journal of Controlled Release

journal homepage: www.elsevier.com/locate/jconrel

Targeting the amyloid-β antibody in the brain tissue of a mouse model of Alzheimer's disease

Daniel McLean [a,b], Michael J. Cooke [a], Yuanfei Wang [a,b], Paul Fraser [c], Peter St George-Hyslop [c,d,e,f,g], Molly S. Shoichet [a,c,h,*]

[a] Department of Chemical Engineering and Applied Chemistry, University of Toronto, Toronto, Ontario, Canada M5S 3E1
[b] Institute of Biomaterials and Biomedical Engineering, University of Toronto, Toronto, Ontario, Canada M5S 3E1
[c] Centre for Research in Neurodegenerative Diseases, University of Toronto, Toronto, Ontario, Canada M5S 3E1
[d] Department of Medicine, University of Toronto, Toronto, Ontario, Canada M5S 3E1
[e] Department of Laboratory Medicine and Pathobiology, University of Toronto, Toronto, Ontario, Canada M5S 3E1
[f] Department of Medical Biophysics, University of Toronto, Toronto, Ontario, Canada M5S 3E1
[g] Cambridge Institute for Medical Research, University of Cambridge, Cambridge CB2 0XY, UK
[h] Department of Chemistry University of Toronto, Toronto, Ontario, Canada M5S 3E1

ARTICLE INFO

Article history:
Received 19 September 2011
Accepted 25 December 2011
Available online 30 December 2011

Keywords:
Diffusion
Elimination
Binding
Amyloid plaque
Antibody specificity
Alzheimer's disease

ABSTRACT

Alzheimer's disease is a neurodegenerative disease characterized pathologically by amyloid-β (Aβ) aggregates in the brain. Notwithstanding many promising therapeutics that are under development, early diagnosis of Alzheimer's disease is limited. By targeting the Aβ aggregates, diagnosis can be improved and disease progression reduced. Molecular imaging using monoclonal antibodies to target specific isoforms of Aβ aggregates offer increased specificity in comparison to conventional imaging tracers; however, antibodies that are widely used in histology do not necessarily show similar binding in a dynamic *in vivo* environment. In this study, the diffusion and binding were studied of a classical monoclonal antibody, 6E10, in the brain of the TgCRND8 mouse model of AD. After intracranial injection of fluorescent 6E10, we observed broad and rapid labelling of Aβ deposits in the cortex and corpus callosum within 4 h. Aβ plaques were detected up to 2.5 mm away from the injection site in TgCRND8 mice and not in wild type mice at all, demonstrating specificity of binding. The apparent diffusivity and elimination constant of the anti-Aβ antibody were found to be independent of both the age of the animal and the accumulation of Aβ in the extracellular space, suggesting broad applicability of this targeting molecule. Mathematical modelling of the diffusion profiles of the anti-Aβ antibody in the brain parenchyma provides insights into the utility of antibodies as molecular imaging tools and targeted therapeutics.

1. Introduction

Alzheimer's disease (AD) is a neurodegenerative disease which impairs cognition, memory and behaviour in 100 million people worldwide, and for which there is no definitive diagnosis or cure [1]. The deposition of amyloid-β (Aβ) protein into neural plaques in the brain parenchyma is considered the hallmark pathological feature of AD [2]. The vast majority of AD therapies target the accumulation of Aβ and for this reason neuroimaging tracers targeting isoforms of Aβ are relevant as diagnostic tools [3].

Monitoring AD patients has traditionally been limited to behavioural observation. More recently computed tomography and magnetic resonance imaging have been introduced to clinical practice to identify ventricular enlargement and cortical atrophy, but these techniques are more useful in the later stages of AD [4]. Positron emission tomography (PET) tracers that can selectively bind to Aβ deposits is a more promising approach as an AD diagnostic tool . The most notable of the PET imaging ligands developed is ^{11}C-Pittsburgh Compound-B (PIB), which is able to clearly distinguish between AD and healthy patients in most cases [5]. Notwithstanding these important results, PIB has also shown both some non-specific binding [6] and limited binding to confirmed AD brain tissue samples [7].

Antibodies have been widely studied in passive immunization and have shown success in clearing Aβ plaques and restoring cognitive function [8]. Peripherally administered polyamine modified anti-Aβ antibodies have bound specifically to Aβ plaques [9]. However, many of the passive immunization studies, using classical monoclonal antibodies such as 6E10, have not demonstrated widespread Aβ plaque labelling despite intracranial delivery [10]. 6E10 is a commercially available monoclonal antibody that is reactive to amino acids 1–16 of Aβ and has been widely used as an immunohistochemical

* Corresponding author at: Terrence Donnelly Center for Cellular and Biomolecular Research, Room 530, 160 College Street, Toronto, Ontario, Canada M5S 3E1. Tel.: +1 416 978 1460; fax: +1 416 978 4317.
E-mail address: molly.shoichet@utoronto.ca (M.S. Shoichet).

0168-3659/$ – see front matter © 2012 Elsevier B.V. All rights reserved.
doi:10.1016/j.jconrel.2011.12.036

reagent [11]. The binding kinetics (association and dissociation constants) of 6E10 have been described in model systems using surface plasmon resonance and are similar to our more physiologically-relevant *in vivo* studies and to some of the binding kinetics of novel antibodies used to label Aβ plaques *in vivo* [12]; however, unlike the present study, none of these studies have examined how the deposition of Aβ in the extracellular space alters the diffusion of antibodies in brain tissue.

The high specificity of antibodies makes antibody-mediated brain imaging in AD an attractive tool that can complement conventional PET tracers [13]. While application of antibodies has typically been limited by low blood–brain barrier permeability and inadequate transport in brain tissue, progress has been made in improving permeability through chemical modification of the antibody [14,15].

Within the larger context of antibody labelling in AD, the primary objective of this study is to visualize and measure the diffusion, binding and elimination of the classical monoclonal antibody, 6E10, in the brain parenchyma of TgCRND8 mice and develop a mathematical model that explains and predicts the diffusion of antibodies in brain tissue. We examine the effect of age and accumulation of Aβ in the extracellular space on the diffusion of antibodies in brain tissue. To avoid confounding issues associated with systemic circulation and blood–brain barrier permeability, 6E10 is injected directly into brain cortical tissue where 6E10 extensively labels Aβ plaques in the TgCRND8 mouse model of AD, but cannot be visualized in the brain of a wild type (WT) mouse. The selective binding observed *in vivo* is further investigated in brain tissue slices using integrative optical imaging (IOI), a technique used to study the diffusion of fluorescently labelled proteins and polymers in the brain [16,17]. Interestingly, the diffusive properties of antibodies in the brain parenchyma of mice is largely unaffected by age and Aβ accumulation. To better elucidate this mechanism of 6E10 antibody diffusion, we developed a mathematical model from first principles that predicts diffusion distance and concentration profiles as a function of time. Understanding how the movement of antibodies through brain tissue is affected by age and accumulation of Aβ in the extracellular space has important implications for the use of antibody therapeutics in AD.

2. Materials and methods

2.1. Mice

Animal experiments were carried out in accordance with the guidelines provided by the Canadian Council for Animal Care and reviewed by an in-house research ethics approval board. TgCRND8 mice were maintained on a 129 background. The TgCRND8 mouse is used as it is widely accepted as a robust model of Aβ deposition [18]. Mice carrying the Swedish and Indiana mutations were differentiated from wild type (WT) mice by PCR analysis of tail DNA.

2.2. Intracranial injection of fluorescent antibody

8 month old mice (TgCRND8 n = 5, WT n = 5) were anaesthetized with isofluorane and placed into a stereotactic apparatus (Kopf). The skull was exposed with an incision and two holes were drilled in the left and right frontal cortex at the following coordinates: rostral: +1 mm, lateral +/−2 mm, relative to bregma. A 26 gauge needle with a 45° bevel tip attached to a 10 μL syringe (Hamilton Company) was used for intracranial injections. Alexa488-6E10 was purchased commercially (Covance Research Products) with approximately two Alexa488 molecules immobilized per IgG. Alexa488 has a molecular weight of 643 g/mol. In comparison the molecular weight of IgG is approximately 150 000 g/mol. As a consequence, the modification of 6E10 with Alexa488 is estimated to have minimal impact on diffusion. The needle and syringe were loaded with Alexa488-6E10 then lowered 1 mm into the left frontal cortex and 0.5 μL of antibody was injected at a rate of 0.1 μL/min. The needle was left in the cortex for 10 min after the injection was completed and removed in 0.2 mm increments over 5 min. For the no antibody control, the needle was lowered 1 mm into the right cortex, left in place for 15 min and then removed in 0.2 mm increments over 5 min. The incision was closed with sutures and the animals left to recover under a heat lamp. Animals were sacrificed 4 h post surgery by CO_2 asphyxiation followed by cervical dislocation.

2.3. Histology

Brains were placed in 4% paraformaldehyde (Sigma-Aldrich) for 12 h at 4 °C, followed by a cryo-protection treatment for 36 h in 30% sucrose (Sigma-Aldrich). Samples were snap-frozen and cut with a cryostat (Leica) into 100 μm thick coronal sections. Slices were viewed with a fluorescent microscope under a FITC filter.

2.4. Immunohistochemistry

Four random coronal sections from the TgCRND8 and WT mice that received Alexa488-6E10 intracranial injections were blocked with 5% bovine serum albumin (Sigma-Aldrich) for 2 h. Sections were stained with a primary rabbit polyclonal anti-amyloid β antibody (1:1000, Abcam Ab2539) for 24 h, followed by staining with an Alexa568 goat anti-rabbit IgG (1:1000, Invitrogen A11003) for 24 h. Vector shield (Vector Laboratories), containing a DAPI nuclear stain, was used to mount sections. Sections were viewed under a spinning disc confocal microscope (Quorum Technologies) with a mercury arc lamp and DAPI filter (excitation filter = 350 nm) and two lasers (excitation = 491 nm and 561 nm).

2.5. Integrative optical imaging (IOI)

IOI techniques were modelled on previous studies. 3, 4, 6, 8 and 16 month-old animals were sacrificed by cervical dislocation, brains harvested and immediately placed into 4 °C artificial cerebrospinal fluid (aCSF) composition of: 124 mM NaCl; 5 mM KCl; 26 mM $NaHCO_3$; 1.25 mM NaH_2PO_4; 1.3 mM $MgCl_2$; 1.5 mM $CaCl_2$; and 10 mM D-(+)-glucose bubbled with 95% O_2/5% CO_2 (pH 7.0). Brains were sectioned using a vibratome into 400 μm thick coronal sections and placed into 4 °C oxygenated aCSF. The diffusion of FITC labelled bovine IgG (Sigma-Aldrich), Alexa488 6E10, and blocked Alexa488 6E10. The 6E10 antibody was blocked by pre-incubating the antibody for 2 h with a 10:1 molar ratio of amyloid β peptide (1–42, Sigma-Aldrich) to 6E10. A microinjector (World Precision Instruments) was used to inject 4 nL of each antibody into the frontal cortex of the 400 μm brain slices. Diffusion of fluorescently labelled antibody was captured using a microscope (Zeiss Axio Observer.Z1) and camera (Hamamatsu ImagEM EMCCD) over a 5 min period. At least 10 injections in 4 slices from 2 different animals were recorded for each antibody in TgCRND8 and WT mice. IOI was also used to estimate free diffusivity of 6E10 in 0.3% agarose.

The apparent diffusivity and first order elimination constant were calculated by using methods described previously [17,19]. ImageJ (http://rsbweb.nih.gov/ij/) was used to quantify the pixel intensity profile at 18 s intervals over the 5 min profile for each injection. Apparent diffusivity and elimination constants were calculated by fitting the intensity profiles to Eqs. (1) and (2) using a programme written in mathCAD v14.0 (PTC). Eq. (1) is used to calculate the apparent diffusivity using early time points where the concentration of protein is high enough to neglect elimination. Eq. (2) is a mass balance of populations of freely diffusing and bound molecules used to calculate diffusivity and a first-order

elimination constant after a point-source injection. Fig. S1, (supplementary information), provides raw data at various points in the analysis to explain how apparent diffusivity and the elimination constant are calculated. Images found in Fig. S1A and B depict representative fluorescent images at 6 early time points taken from 8 month old transgenic and wild-type animals. Pixel intensity was plotted *versus* pixel distance for each of these representative images and is shown in Fig. S1C and D. These profiles were fitted to Eq. (1) and the gamma term extracted for each profile and plotted as a function of time, shown in Fig. S1E and F. Only fits with R-squares greater than 0.8 were accepted. At early time points, the change in gamma over time is linear and the slope equal to apparent diffusivity. Once apparent diffusivity was calculated, Eq. (2) was fitted to the intensity profiles and the elimination constant extracted. In the absence of elimination, the fluorescent profile will eventually fade to background as the fluorophore reaches concentrations below the detection limit. In the presence of elimination, eventually all fluorophores are immobilized and the fluorescent profile does not change. IOI uses this principle to separate elimination from apparent diffusivity. $I(r,t)$ is the pixel intensity at distance r from injection site and time t after injection, r is the radial distance from injection site (cm), E is the de-focused point-spread function of objective [19], t is the time after injection (s), D_A is the apparent diffusivity (cm^2/s), k_e is elimination constant (s^{-1}), ε is the fluorophore efficiency upon cellular internalization, I_0 is the initial fluorescent intensity, U is the volume of protein injected, C_p is the concentration of the protein solution, and α is the volume fraction of extracellular matrix in the brain. Since the time required for internalization exceeded the time scale of IOI [17], the fluorophore efficiency was deemed to be united. The volume fraction was estimated at 0.2 [17].

$$I(r,y) = E\cdot \exp\left(-\left(\frac{r}{\gamma}\right)^2\right), \gamma = (4D(t+t_o))^{\frac{1}{2}} \quad (1)$$

$$I(r,t) = \frac{I_o U C_p}{\alpha(4\pi D_A t)^{3/2}}\cdot \exp\left(\frac{-r^2}{4D_A t}\right)\cdot \exp(-k_e(t-t_0)) + \varepsilon\cdot I_0 k_e \cdot \int_{t_0}^{t} \frac{UC_p}{\alpha(4\pi D_A t)^{3/2}}\cdot \exp\left(\frac{-r^2}{4D_A t}\right)\cdot \exp(-k_e(t-t_0))dt \quad (2)$$

3. Results

3.1. Alexa488-6E10 diffusion and elimination in 8 month old TgCRND8 mice

Four hours after intracranial injection of Alexa488-labelled 6E10 into 8 month old TgCRND8 mice, numerous fluorescent deposits were observed in the left (ipsilateral) hemisphere demonstrating that 6E10 binds to Aβ plaques (Fig. 1A). Deposits range in size from less than 1 μm to 15 μm in diameter and are distributed up to 2.5 mm from the injection site, including around the needle track. In contrast, no fluorescent deposits are observed near the needle track on the control right hemisphere (data not shown). Similarly, fluorescent deposits are not observed in the wild type animals injected with 6E10 (Fig. 1B). Together, these data demonstrate the specificity of 6E10 antibody binding to Aβ plaques in live animals, thereby advancing a histological technique towards a diagnostic tool.

The distribution of the fluorescent deposits on a global scale was investigated by examining complete brain sections surrounding the injection site. Fluorescent deposits are widely distributed throughout the brain parenchyma in sections taken 1 mm rostral to the injection site (Fig. 2A). Sections taken from the injection site contain deposits surrounding the injection site throughout the cortex and along the corpus callosum (Fig. 2B). Brain sections taken 1 mm caudal to the injection site had fluorescent deposits predominantly located along the corpus callosum (Fig. 2C). In contrast, brain sections rostral and caudal to the injection site in the wild type animal contain no fluorescent deposits (Fig. 2D,E,F).

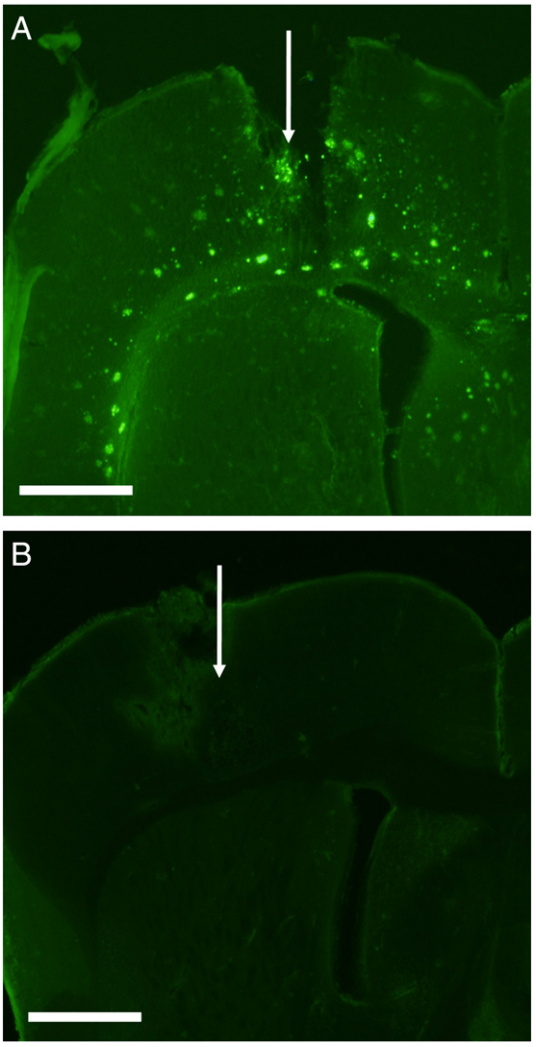

Fig. 1. Alexa488-6E10 binds to plaques in 8 month old TgCRND8 mice. Numerous, large fluorescent deposits are found several millimetres away from an intracortical (0.5 μL) injection of Alexa488-6E10 anti-amyloid β antibody in TgCRND8 mice. (A) 6E10 antibody is immobilized in large deposits surrounding the needle track and on both sides of the lateral ventricle (n = 5; 1.25× magnification, scale bar 1 mm). (B) No Alexa488-6E10 antibody is found in the brain of a wild type animal (n = 5; 1.5× magnification, scale bar 1 mm). White arrow indicates the injection site.

The shape and morphology of the individual fluorescent deposits in the TgCRND8 mice were examined using confocal microscopy. Confocal images taken at 2 μm increments through a representative fluorescent deposit 15 μm in diameter show a round, fibrous and hollow morphology (Fig. 3), reflecting the shape of previously reported 6E10-stained Aβ plaques [12,20]. This is the first demonstration of live animal labelling of Aβ plaques with 6E10 — previous staining with 6E10 used histological techniques.

3.2. Counter staining Alexa488-6E10 deposits with rabbit polyclonal anti-amyloid β antibody

To confirm that the fluorescent deposits observed in the transgenic animals were Aβ plaques, the sections were stained with a rabbit polyclonal anti-amyloid β IgG and a secondary detection antibody. In most fluorescent deposits, the polyclonal anti-amyloid β IgG (Fig. 4A) overlapped convincingly with the 6E10

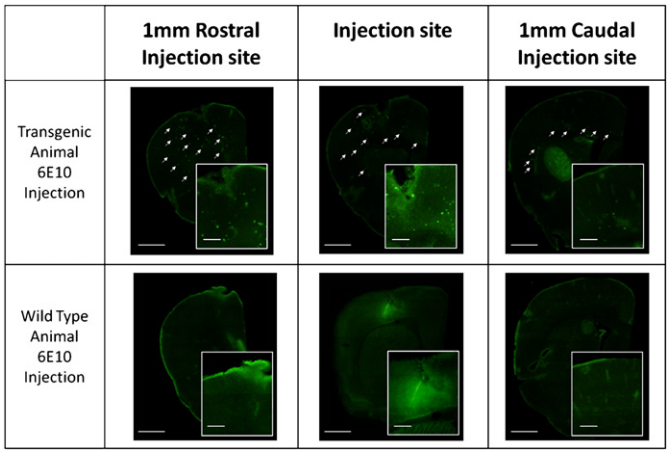

Fig. 2. Distribution of Alexa488-6E10 illuminated plaques in TgCRND8 mice. Alexa488-6E10 anti-amyloid β antibody binds to senile plaques in TgCRND8 mice, while no antibody is retained in the wild type mice after intracortical injections (0.5 μL). White arrows indicate fluorescent deposits that are found several millimetres from the injection site. Inset images show a close-up of the injection site where many fluorescent deposits are found. No fluorescence was observed on the control side of brains (scale bar 1 mm, inset scale bar 250 μm).

deposit (Fig. 4B). Overlaying the two images (Fig. 4C) shows that the polyclonal IgG stains the core of the senile plaque while 6E10 binds mostly to the periphery. The DAPI nuclear stain (Fig. 4D) did not colocalize with either the 6E10 deposits or the polyclonal anti-amyloid β IgG, demonstrating that the 6E10 deposits are extracellular as would be expected of senile plaques (Fig. 4C). In these images, *in vivo* labelling of 6E10 appears to stain the periphery of Aβ plaques, showing the characteristic halo pattern whereas in immunohistochemical staining, the polyclonal antibody penetrates deeper into the core of the Aβ plaques, demonstrating typical even staining. We attribute this difference to the distinct binding conditions (*in vivo versus* histological) and the broader binding of the polyclonal antibody.

3.3. Antibody diffusion and elimination from TgCRND8 versus WT brain parenchyma

To gain greater insight into the kinetics of 6E10 diffusion in brain tissue, IOI was used to assess diffusion of the antibody through the brain parenchyma: the brain tissue from animals of 5 different ages was compared from WT and TgCRND8 animals. Apparent diffusivity of 6E10 was estimated at 3×10^{-7} cm^2/s by fitting IOI data to Eq. (1). Apparent diffusivity of 6E10 is statistically indistinguishable regardless of the age of the animal and the presence of Aβ in the brain parenchyma (Fig. 5A). Free diffusivity of 6E10 was estimated in a dilute agarose solution (0.3%) at 5.8 cm^2/s, which is roughly twice as fast as in the brain tissue.

The first order elimination constant was calculated by fitting IOI data to Eq. (2). The elimination constant encompasses all the mechanisms by which a freely diffusing molecule is no longer diffusing and largely depends on that molecule being immobilized (binding to chemical receptors, nonspecific binding to

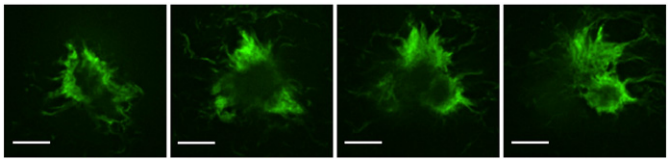

Fig. 3. Individual Alexa488-6E10 deposits have fibrous, hollow morphology. Confocal image slices (2 μm apart) of the Alexa488-6E10 deposits found in the brains of TgCRN8 mice after the intracranial injection (63× magnification, scale bar 7 μm).

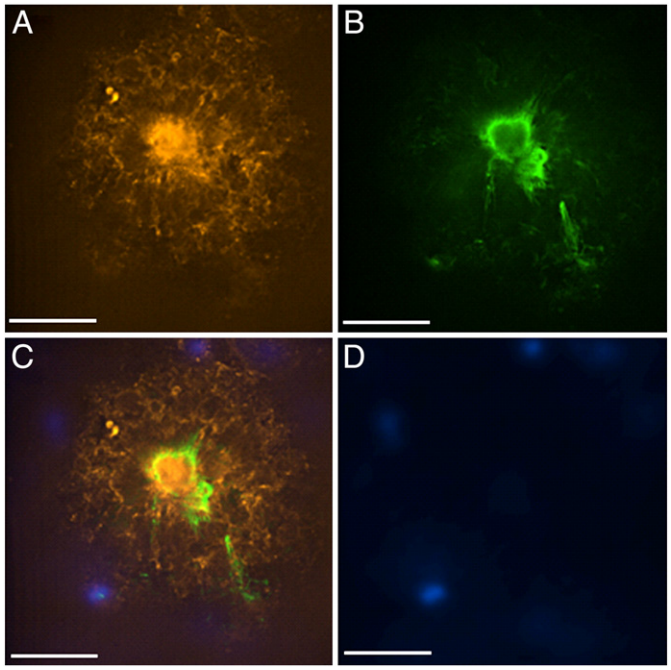

Fig. 4. Alexa488-6E10 deposits are composed of Aβ. Immunohistological staining with a rabbit polyclonal anti-amyloid β antibody reveals co-localization with the Alexa488-6E10 deposits observed after intracranial injections. (A) Illumination using a 561 nm laser illustrates a senile plaque stained by rabbit polyclonal anti-amyloid β antibody (63× magnification, scale bar 20 μm). (B) Illumination using a 491 nm laser of a representative Alexa488-6E10 deposit displays the characteristic halo-like pattern (63× magnification, scale bar 20 μm). (C) Merged image of Alexa488-6E10 anti-amyloid β deposit and Alexa568 anti-rabbit antibody shows overlap indicating that 6E10 deposits are senile plaques (63× magnification, scale bar 20 μm). (D) DAPI channel reveals senile plaque deposits are not associated with cell nuclei (63× magnification, scale bar 20 μm).

extracellular matrix, *etc.*) and no longer moving through the extracellular space. Degradation would normally also contribute to elimination; however, the IOI studies are too short for degradation to be of concern. Elimination was unaffected by the age of the WT animal, indicating that age-related changes in the extracellular space do not affect immobilization (Fig. 5B). The elimination constant remained similar at all ages in TgCRND8 mice, with the exception of the 4 month old animals. There is a significant increase in total amount of antibody bound at 4 months of age relative to other age cohorts and the WT animal. In order to understand whether the elevated binding was due to the accumulation of Aβ in the extracellular space, a control was carried out where the antigen binding site on 6E10 was blocked through pre-incubating the antibody with an Aβ peptide to block specific binding. Importantly, by blocking the active site of 6E10, the increased elimination constant at 4 months of age is in line with typical levels, confirming the specificity and validity of this methodology to quantify specific binding interactions.

4. Discussion

In contrast to previous reports, intracranial injection of 6E10 into the cortex of TgCRND8 mice was able to label Aβ plaques surrounding the injection site, as far away as 2.5 mm [10]. The shape, size and morphology of the fluorescent deposits combined with the co-labelling with a polyclonal anti-Aβ antibody demonstrate that these deposits are composed of Aβ. An effective diagnostic imaging tool (or a therapeutic) must permeate the entire tissue, bind specifically with the target and clear rapidly from non-targeted tissue. The binding of 6E10 to senile plaques is important because the antibody was able to penetrate the brain tissue of TgCRND8 mice in only 4 h and

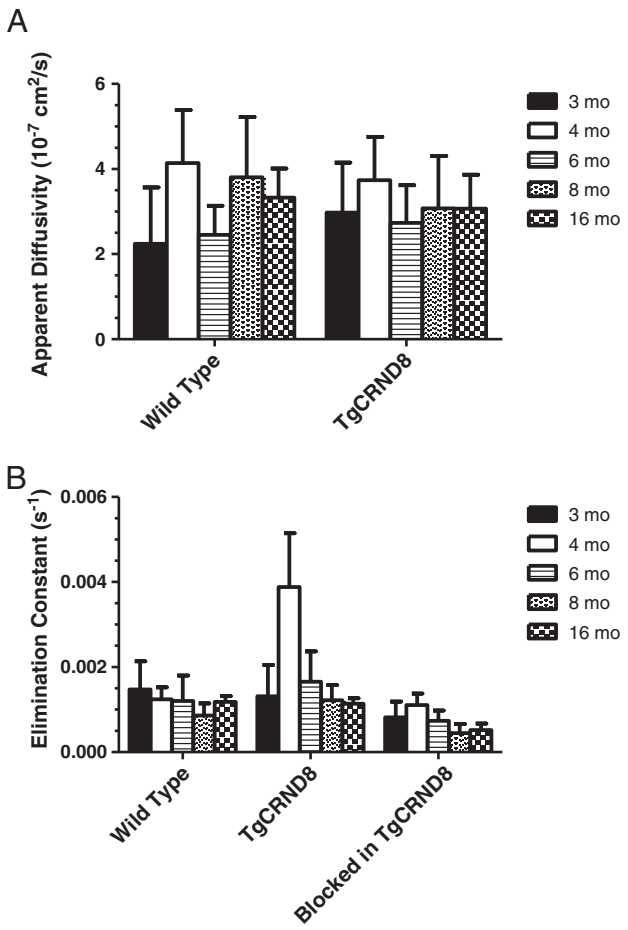

Fig. 5. Apparent diffusivity and elimination is largely unaffected by age and accumulation of Aβ. Calculating the apparent diffusivity and first-order elimination constant of Alexa488-6E10 anti-amyloid β in TgCRND8 mouse brain tissue reveals that this antibody diffuses readily and is quickly bound. (A) Apparent diffusivity (cm^2/s) of Alexa488-6E10 in wild type and TgCRND8 mouse brain tissue is not significantly affected by the age of the animal. (B) First-order elimination constant reveals a similar level of binding at all ages in the wild type, while in the TgCRND8 mouse the binding is elevated at 4 months of age. After blocking the antigen binding site of 6E10, by preincubating with amyloid β peptide, the elimination of the 6E10 antibody is significantly reduced in the transgenic animal. Apparent diffusivity and first-order elimination constants were calculated by fitting IOI data to Eq. (2).

is visually different from that in wild type tissue (see Fig. 1). Importantly, unbound antibody could not be visualized in the parenchyma at this short time period. We estimated that all plaques within 2 mm of the injection site were labelled, assuming isotropic diffusion. Based on previous studies by Zhang and Sejnowski on volume of the cortex, [21], we estimate that approximately 66% of all plaques in the cortex were labelled. We can further refine our estimate, based on studies by Dudal et al. [20] who suggested that 60% of plaques are located in the cortex, to approximately 40% of the plaques present in the left side of the brain being labelled with 6E10. Thus intracranial injection of 6E10 can provide a broad, unbiased assessment of the Aβ content in the cortex tissue of the TgCRND8 mouse model, but cannot measure Aβ content in other areas of the brain such as the hippocampus.

The pattern of Aβ plaque labelling in the TgCRND8 brain tissue suggests the presence of both convective and diffusive mass transfer. In brain slices rostral to the injection site, 6E10 diffused radially away from the injection site. The broad pattern of distribution in the rostral tissue suggests diffusive mass transfer as the antibody seemed to move randomly through the brain rather than along a defined path. No evidence of convective mass transfer in this part of the brain could be found in the literature, which strengthens the hypothesis that the staining in this region is predominantly an effect of diffusive mass transfer. In contrast, convective mass transfer is likely responsible for antibody diffusion around the injection site as the antibody clearly diffused more readily through the corpus callosum than the cortex, as evidenced by the larger diffusion distances observed and limited staining in the cortex. Similarly, tissue caudal to the injection site only contained fluorescent plaques along the corpus callosum and not along the cortex, indicating that the antibody preferentially moved in this direction. Studies of the movement of macromolecules in the rat brain have confirmed convective mass transfer along the corpus callosum [22], which agrees with our observations.

Widespread labelling of Aβ plaques throughout the cortex and corpus callosum with 6E10 contrasts with other reports [10,23–25]. At 4 h after injection, Wilcock et al. noted limited staining of Aβ plaques in the Tg2576 mouse model and that 6E10 remained localized to the area of injection for up to 1 week. We suggest three experimental differences to account for the increased 6E10 binding to Aβ plaques observed in our studies. (1) The TgCRND8 mouse model deposits Aβ plaques more quickly than the Tg2576 mouse model. Comparing 8 month old TgCRND8 mice to 16 month old Tg2576 mice is difficult as different amounts and types of Aβ may be present in each animal. (2) Our injection techniques differed as we left the needle in place for a much longer period of time in order to minimize antibody backflow. (3) We did not use a secondary antibody to detect the location of the injected 6E10, but instead traced its diffusion directly with a primary label. A primary label enhances the selectivity of detection. The differences are significant from a diagnostic point of view because 6E10 may be a more valuable tool for labelling plaques *in vivo* than was previously suggested.

To more fully understand the large diffusion distances and rapid clearance we observed after intracranial injection of 6E10, the apparent diffusivity and elimination constants of 6E10 were measured. Apparent diffusivity and elimination constant were measured with IOI and describe the tissue environment on a scale that is much smaller than that examined after intracranial injection of 6E10. In contrast to the intracranial injection where the entire brain was observed over 4 h, IOI describes the movement of 6E10 through the extracellular space over much smaller distances (400 μm) and time frames (4 min). The apparent diffusivity of 6E10 in TgCRND8 and WT mice was consistent across all ages. Aβ plaques, while plentiful on a global scale [18], only account for a small fraction of the elimination on the small scale in which the elimination constant is measured. This observation has important consequences in imaging applications, as the diffusion of 6E10 through the brain parenchyma will not be biassed by the age of the animal or the accumulation of Aβ. The determining factor for the retention of 6E10 in the brain is the antigen to which it binds, rather than non-specific changes in the extracellular environment.

Despite the clear binding of 6E10 to Aβ plaques observed after intracranial injections, it appears that ageing or accumulation of Aβ plaques does not change the extracellular space in a way that affects the diffusion and elimination of 6E10. This observation is consistent with existing literature that has shown that elimination and diffusion of macromolecules in aged and AD tissue remain unaffected. The extracellular space volume fraction is known to decrease as wild type animals age, mostly due to the loss of extracellular matrix [26]. In contrast, the extracellular space volume fraction of APP23 mice increases as Aβ is deposited in the parenchyma, presumably due to neuronal loss [27]. Reduced numbers of neurons and axons have been described in the TgCRND8 mice, suggesting that increased extracellular space volume fraction would be expected as was documented in APP23 mice [28]. These counterbalancing effects could explain why the apparent diffusivity of antibodies is unaffected by the age of the animal and the accumulation of Aβ in the extracellular space in TgCRND8 mice.

There is evidence of increased extracellular volume fraction that is not accompanied by changes in apparent diffusivity [29]. However, conflicting reports have shown that fluorescent 70 kDa dextran can diffuse more quickly when the extracellular volume fraction increases [30]. Our evidence supports the hypothesis that increased extracellular volume fraction has a limited impact on apparent diffusivity, but it is important to note that the extracellular environment can vary dramatically in different mouse models and the diffusing molecules all have different shapes, sizes and charges.

6E10 elimination from the extracellular space remained largely independent of the animal age and accumulation of Aβ, with the exception of the 4 month old TgCRND8 mice. We expected to see some differences in elimination when comparing TgCRND8 to WT mice because Aβ deposits can account for up to 20% of the brain volume in some mouse models of AD [27]. Non-specific binding of 6E10 to the extracellular molecules is likely responsible for the bulk of the elimination constant observed using IOI relative to the influence of Aβ deposits. Removal of an IgG molecule from brain tissue first requires binding to an extracellular molecule that facilitates efflux from the brain. In the case of 6E10, its rapid clearance from the WT mouse by 4 h, indicates a high level of non-specific binding in the extracellular space.

At 4 months of age, elimination from the extracellular space of TgCRND8 mice was elevated approximately 3.5 fold over the WT control and all other ages examined in the TgCRND8. The elimination constant was restored to control levels by blocking the antigen binding site. Changes in Aβ levels at 4 months of age in the TgCRND8 are implicated in the significant rise in elimination. Multiple Aβ species are present in different concentrations over the lifespan of transgenic models of AD [31]. A widely dispersed, diffuse species of Aβ might be present at 4 months of age that is responsible for elevating the elimination constant of 6E10 in this animal cohort.

We developed a mathematical model that is able to predict concentration profiles as a function of both distance from injection site and time after injection and can be found in the supplementary information. Mathematical modelling of the diffusion and elimination of 6E10 in the extracellular space provides important insight into the utility of antibodies as imaging tools (and potential therapeutics). Antibody concentrations reach a local maximum within 3 h in the regions of the brain where Aβ plaque labelling was observed. The local maximum likely reflects labelling of the plaque, followed by a decrease in the background concentration of the antibody which allows the plaque to be visualized. Consequently, individual plaques can be differentiated from background. Also, the rapid removal of antibody observed in the WT mouse is consistent with the antibody concentrations predicted by the model. This model is not only useful in understanding our *in vivo* observations, but can be used to optimize administration parameters to achieve specific biological aims such as dose or volume of distribution.

To assess the translation of these results from a mouse model to clinical applications, we predicted the maximum distance a plaque could be labelled in a human brain using the mathematical model. The threshold plaque-labelling antibody concentration was estimated to be the maximum concentration reached 3 mm from the injection site in the TgCRND8 mouse, which from our model was approximately 1×10^{-12} mg/mL. We optimized the injection conditions in our model by increasing the volume of injection (3 μL) and the antibody concentration (10 mg/mL); however, the concentration of antibody in the tissue did not rise above the threshold. These calculations suggest that intracortical delivery of an antibody will not penetrate far enough in the human brain; however, this analysis assumes that the elimination constant cannot be reduced and relates only to intracortical delivery. The elimination of a monoclonal antibody may be reduced by removing the Fc region or using single chain binding proteins [32]. A reduced elimination constant would increase the penetration distance of an antibody. Moreover, modifications to the antibody or the blood–brain barrier would allow intravenous delivery. Since the brain is highly vascularised, diffusion distances of 3 mm from the brain vasculature would reach the Aβ plaques, demonstrating the potential for translation of antibody labelling.

Interestingly, 6E10 has been widely reported to reduce Aβ deposition, indicating that 6E10 can be used as both a molecular imaging tool and a targeted therapeutic [33]. It has been proposed that much of the therapeutic benefit of classical monoclonal antibodies is mediated through the Fc receptor [32]. In diagnostic and monitoring applications, where it is important to separate diagnosis from therapeutic, removal of the Fc region of monoclonal antibodies may provide a mechanism to retain molecular targeting of antibodies without influencing disease progression.

Intracortical injection of the 6E10 monoclonal antibody rapidly and specifically labels Aβ plaques that allow TgCRND8 and WT mice to be clearly differentiated. Age-related or Aβ-induced changes in the morphology of brain tissue do not appear to affect the apparent diffusion of 6E10 in the extracellular space. Similarly, age and Aβ deposition have limited impact on the elimination of 6E10 from the extracellular space of this mouse model. The data presented here provide a framework for live animal PET imaging in the future where a PET isotope can be used to non-invasively measure the retention of 6E10 in the mouse brain. Moreover, non-invasive imaging will need to be coupled with non-invasive delivery of the antibody to the cortex, such as intravenous delivery with a permeabilizing strategy for the blood–brain barrier or chemically modifying the antibody to increase permeability [15]. Clearly, antibodies remain an excellent tool in the treatment, diagnosis and monitoring of AD because of their ability to target specific isoforms of Aβ and these results facilitate their transition from histological technique to diagnostic tool. These results also have broad implications where antibodies or antibody–drug conjugates are required to diffuse through brain tissue in other disease models.

Acknowledgements

The authors gratefully acknowledge the technical expertise of Rosemary Ahrens (Centre for Research in Neurodegenerative Diseases, University of Toronto) and Bruno Chue (Centre for Biological Timing and Cognition) and helpful discussions with David Green (Spatio-Temporal Targeting and Amplification of Radiation Response). DM acknowledges the Vanier Canada Graduate Scholarship programme, MC acknowledges the Ontario Neurotrauma Foundation post-doctoral fellowship and YW acknowledges the Natural Sciences and Engineering Research Council Canadian Graduate Scholarship (CGSD). Work was funded by a Firefly Foundation Grant (to PSGH, PF) and the Natural Sciences and Engineering Research Council of Canada (to MSS).

Appendix A. Supplementary data

Supplementary data to this article can be found online at doi:10.1016/j.jconrel.2011.12.036.

References

[1] J.L. Holtzman, Are we prepared to deal with the Alzheimer's disease pandemic? Clin. Pharmacol. Ther. 88 (2010) 563–565.
[2] R. Katzman, Alzheimer's disease, N. Engl. J. Med. 314 (1986) 964–973.
[3] D.A. Wolk, W.E. Klunk, Update on amyloid imaging: from healthy aging to Alzheimer's disease, Curr. Neurol. Neurosci. Rep. 9 (2009) 345–352.
[4] D.S. Knopman, S.T. DeKosky, J.L. Cummings, H. Chui, J. Corey-Bloom, N. Relkin, G.W. Small, B. Miller, J.C. Stevens, Practice parameter: diagnosis of dementia (an evidence-based review) — report of the Quality Standards Subcommittee of the American Academy of Neurology, Neurology 56 (2001) 1143–1153.
[5] J. Shin, S.Y. Lee, S.J. Kim, S.H. Kim, S.J. Cho, Y.B. Kim, Voxel-based analysis of Alzheimer's disease PET imaging using a triplet of radiotracers: PIB, FDDNP, and FDG, Neuroimage 52 (2010) 488–496.

[6] J.O. Rinne, D.J. Brooks, M.N. Rossor, N.C. Fox, R. Bullock, W.E. Klunk, C.A. Mathis, K. Blennow, J. Barakos, A.A. Okello, S.R.M. de Llano, E. Liu, M. Koller, K.M. Gregg, D. Schenk, R. Black, M. Grundman, C-11-PiB PET assessment of change in fibrillar amyloid-beta load in patients with Alzheimer's disease treated with bapineuzumab: a phase 2, double-blind, placebo-controlled, ascending-dose study, Lancet Neurol. 9 (2010) 363–372.
[7] T. Suotunen, J. Hirvonen, P. Immonen-Raiha, S. Aalto, I. Lisinen, E. Arponen, M. Teras, K. Koski, R. Sulkava, M. Seppanen, J.O. Rinne, Visual assessment of C-11 PIB PET in patients with cognitive impairment, Eur. J. Nucl. Med. Mol. Imaging 37 (2010) 1141–1147.
[8] C. Janus, J. Pearson, J. McLaurin, P.M. Mathews, Y. Jiang, S.D. Schmidt, M.A. Chishti, P. Horne, D. Heslin, J. French, H.T.J. Mount, R.A. Nixon, M. Mercken, C. Bergeron, P.E. Fraser, P. St George-Hyslop, D. Westaway, A beta peptide immunization reduces behavioural impairment and plaques in a model of Alzheimer's disease, Nature 408 (2000) 979–982.
[9] M. Ramakrishnan, T.M. Wengenack, K.K. Kandimalla, G.L. Curran, E.J. Gilles, M. Ramirez-Alvarado, J. Lin, M. Garwood, C.R. Jack, J.F. Poduslo, Selective contrast enhancement of individual Alzheimer's disease amyloid plaques using a polyamine and Gd-DOTA conjugated antibody fragment against fibrillar A beta 42 for magnetic resonance molecular imaging, Pharm. Res. 25 (2008) 1861–1872.
[10] D.M. Wilcock, G. DiCarlo, D. Henderson, J. Jackson, K. Clarke, K.E. Ugen, M.N. Gordon, D. Morgan, Intracranially administered anti-A beta antibodies reduce beta-amyloid deposition by mechanisms both independent of and associated with microglial activation, J. Neurosci. 23 (2003) 3745–3751.
[11] S. Funamoto, M. Morshima-Kawashima, Y. Tanimura, N. Hirotani, T.C. Saido, Y. Ihara, Truncated carboxyl-terminal fragments of beta-amyloid precursor protein are processed to amyloid beta-proteins 40 and 42, Biochemistry 43 (2004) 13532–13540.
[12] M. Ramakrishnan, K.K. Kandimalla, T.M. Wengenack, K.G. Howell, J.F. Poduslo, Surface plasmon resonance binding kinetics of Alzheimer's disease amyloid beta peptide-capturing and plaque-binding monoclonal antibodies, Biochemistry 48 (2009) 10405–10415.
[13] M. Ramakrishnan, G.L. Curran, E.J. Gilles, T.M. Wengenack, M. Ramirez-Alvarado, J.F. Poduslo, Development of antibody fragments as contrast agents for the magnetic resonance molecular imaging of Alzheimer's amyloid plaques, Amyloid-J. Protein Fold. Disord. 13 (2006) 54.
[14] J.F. Poduslo, G.L. Curran, J.A. Peterson, D.J. McCormick, A.H. Fauq, M.A. Khan, T.M. Wengenack, Design and chemical synthesis of a magnetic resonance contrast agent with enhanced in vitro binding, high blood–brain barrier permeability, and *in vivo* targeting to Alzheimer's disease amyloid plaques, Biochemistry 43 (2004) 6064–6075.
[15] J.F. Poduslo, M. Ramakrishnan, S.S. Holasek, M. Ramirez-Alvarado, K.K. Kandimalla, E.J. Gilles, G.L. Curran, T.M. Wengenack, *In vivo* targeting of antibody fragments to the nervous system for Alzheimer's disease immunotherapy and molecular imaging of amyloid plaques, J. Neurochem. 102 (2007) 420–433.
[16] C. Nicholson, L. Tao, Hindered diffusion of high-molecular-weight compounds in brain extracellular microenvironment measured with integrative optical imaging, Biophys. J. 65 (1993) 2277–2290.
[17] Y.F. Wang, M.J. Cooke, Y. Lapitsky, R.G. Wylie, N. Sachewsky, D. Corbett, C.M. Morshead, M.S. Shoichet, Transport of epidermal growth factor in the stroke-injured brain, J. Control. Release. 149 (2011) 225–235.
[18] M.A. Chishti, D.S. Yang, C. Janus, A.L. Phinney, P. Horne, J. Pearson, R. Strome, N. Zuker, J. Loukides, J. French, S. Turner, G. Lozza, M. Grilli, S. Kunicki, C. Morissette, J. Paquette, F. Gervais, C. Bergeron, P.E. Fraser, G.A. Carlson, P. St George-Hyslop, D. Westaway, Early-onset amyloid deposition and cognitive deficits in transgenic mice expressing a double mutant form of amyloid precursor protein 695, J. Biol. Chem. 276 (2001) 21562–21570.
[19] R.G. Thorne, S. Hrabetova, C. Nicholson, Diffusion of epidermal growth factor in rat brain extracellular space measured by integrative optical imaging, J. Neurophysiol. 92 (2004) 3471–3481.
[20] S. Dudal, P. Krzywkowski, J. Paquette, C. Morissette, D. Lacombe, P. Tremblay, F. Gervais, Inflammation occurs early during the A[beta] deposition process in TgCRND8 mice, Neurobiol. Aging 25 (2004) 861–871.
[21] K. Zhang, T.J. Sejnowski, A universal scaling law between gray matter and white matter of cerebral cortex, Proc. Natl. Acad. Sci. U. S. A. 97 (2000) 5621–5626.
[22] S.S. Prabhu, W.C. Broaddus, G.T. Gillies, W.G. Loudon, Z.J. Chen, B. Smith, Distribution of macromolecular dyes in brain using positive pressure infusion: a model for direct controlled delivery of therapeutic agents, Surg. Neurol. 50 (1998) 367–375.
[23] D.M. Wilcock, P.T. Jantzen, Q. Li, D. Morgan, M.N. Gordon, Amyloid-beta vaccination, but not nitro-nonsteroidal anti-inflammatory drug treatment, increases vascular amyloid and microhemorrhage while both reduce parenchymal amyloid, Neuroscience 144 (2007) 950–960.
[24] D.M. Wilcock, S.K. Munireddy, A. Rosenthal, K.E. Ugen, M.N. Gordon, D. Morgan, Microglial activation facilitates A beta plaque removal following intracranial anti-A beta antibody administration, Neurobiol. Dis. 15 (2004) 11–20.
[25] S.M.F. Tucker, D.R. Borchelt, J.C. Troncoso, Limited clearance of pre-existing amyloid plaques after intracerebral injection of A beta antibodies in two mouse models of Alzheimer disease, J. Neuropathol. Exp. Neurol. 67 (2008) 30–40.
[26] D.N. Abrous, M.F. Montaron, K.G. Petry, G. Rougon, M. Darnaudery, M. LeMoal, W. Mayo, Decrease in highly polysialylated neuronal cell adhesion molecules and in spatial learning during ageing are not correlated, Brain Res. 744 (1997) 285–292.
[27] E. Sykova, I. Vorisek, T. Antonova, T. Mazel, M. Meyer-Luehmann, M. Jucker, M. Hajek, M. Or, J. Bures, Changes in extracellular space size and geometry in APP23 transgenic mice: a model of Alzheimer's disease, Proc. Natl. Acad. Sci. U. S. A. 102 (2005) 479–484.
[28] A. Bellucci, F. Luccanini, C. Scali, C. Prosperi, M. Grazia Giovannini, G. Pepeu, F. Casamenti, Cholinergic dysfunction, neuronal damage and axonal loss in TgCRND8 mice, Neurobiol. Dis. 23 (2006) 260–272.
[29] X.M. Yao, S. Hrabetova, C. Nicholson, G.T. Manley, Aquaporin-4-deficient mice have increased extracellular space without tortuosity change, J. Neurosci. 28 (2008) 5460–5464.
[30] Z. Zador, M. Magzoub, S. Jin, G.T. Manley, M.C. Papadopoulos, A.S. Verkman, Microfiberoptic fluorescence photobleaching reveals size-dependent macromolecule diffusion in extracellular space deep in brain, FASEB J. 22 (2008) 870–879.
[31] G.M. Shankar, M.A. Leissring, A. Adame, X.Y. Sun, E. Spooner, E. Masliah, D.J. Selkoe, C.A. Lemere, D.M. Walsh, Biochemical and immunohistochemical analysis of an Alzheimer's disease mouse model reveals the presence of multiple cerebral A beta assembly forms throughout life, Neurobiol. Dis. 36 (2009) 293–302.
[32] R. Deane, A. Sagare, K. Hamm, M. Parisi, B. LaRue, H.A. Guo, Z.H. Wu, D.M. Holtzman, B.V. Zlokovic, IgG-assisted age-dependent clearance of Alzheimer's amyloid beta peptide by the blood–brain barrier neonatal Fc receptor, J. Neurosci. 25 (2005) 11495–11503.
[33] D.L. Morse, R.J. Gillies, Molecular imaging and targeted therapies, Biochem. Pharmacol. 80 (2010) 731–738.